



Forming Highly Polluted PMs Caused by the Invasion of Transboundary Air Pollutants: Model Simulation and Discussion

Chung-Hsuang Hung¹, Kuo-Cheng Lo^{2*}, Chung-Shin Yuan³

¹ Department of Safety, Health, and Environmental Engineering, National Kaohsiung University of Science and Technology, Kaohsiung 82445, Taiwan

² Department of Military Meteorology, Air Force Institute of Technology, Kaohsiung 82047, Taiwan

³ Institute of Environmental Engineering, National Sun Yat-Sen University, Kaohsiung 80424, Taiwan

ABSTRACT

Transboundary air pollutants that deteriorate ambient air quality have become an emerging international concern recently. This study analyzed and simulated an air pollution case of highly concentrated particulate matter (PM) formed by a severe dust storm case from January 17 till 19 in 2014. For this case, concentrations of PM₁₀ and PM_{2.5} reached up to 680 and 165 $\mu\text{g m}^{-3}$, respectively. Those concentrations were 5–10 folds higher than the proposed ambient air quality standards of Taiwan. The mechanisms for forming high-concentrated PM in the ambient air of Taiwan and its surrounding area were investigated. Based on the monitored pollutant concentrations and the simulation results with the Weather Research and Forecasting-Chemistry (WRF-Chem) model, both the meteorological conditions and the mechanisms for forming high-concentrated PMs were analyzed. The long-range transported-in air pollutants, travelling with the movement of a strong continental cold high-pressure system originating in northern China, contributed to the poor ambient air quality. Two important mechanisms for forming this highly concentrated PM were proposed, including the transported-in transboundary air pollutants (or their precursors) from China and the leeward side effects on the western side of the Taiwan Island. Low inversion layers in the atmosphere and terrain downwash near the ground surface were observed in this case study while continental cold air approached. The WRF-Chem model simulation results confirmed that the ambient air of western Taiwan was dry and moved downward during the investigated period. Hence, the contribution of transboundary air pollutants to deteriorating ambient air quality cannot be ignored.

Keywords: Transboundary air pollutants; WRF-Chem; PM_{2.5}; PM₁₀; Haze case.

INTRODUCTION

The air pollution problems caused by the invasion of transboundary air pollutants have become problems of universal concern because the movements of transboundary air pollutants are mostly uncontrollable (Zheng *et al.*, 2005; Nenes *et al.*, 2011; Gao *et al.*, 2014; Wang *et al.*, 2015; Liu *et al.*, 2016; Wang *et al.*, 2017). The pollution problems induced by transboundary air pollutants were less crucial in the past, but the problems have become more serious recently due to global climate change. Extreme climate events not only alter the weather patterns but also transfer air pollutants farther from their origins (Fiore *et al.*, 2012; Fang *et al.*, 2013; Li *et al.*, 2013; Zhang *et al.*, 2014; Donkelaar *et al.*, 2015).

Poor air quality is of great concern to the residents of

western Taiwan from late autumn till early spring, particularly. Particulate matters (PMs) are major concerned air pollutants with concentrations above the ambient air quality standards (Hung and Lo, 2015; Li *et al.*, 2015; Wu *et al.*, 2015). Highly concentrated PM cases are often observed from late autumn till early spring in Taiwan, which are mainly caused by two important reasons, including heavy loading of air pollutants originally and unfavorable meteorological conditions for air pollutants dispersing in the ambient air within these periods (Lu *et al.*, 2006; Yen *et al.*, 2013; Zhang *et al.*, 2017), especially for the latter reason. Atmospheric subsidence over western Taiwan is commonly observed with “northeastern monsoon winds” blowing toward Taiwan, which typically occurs during the periods from late autumn till early spring. In compassion of reducing emissions of local air pollutants, it is much more difficult to constrain the invasion of transboundary air pollutants, and less investigation was conducted for this kind of transport-in pollution problems. Thus, clarifying the forming reason is necessary.

Both air quality and meteorological models are often

* Corresponding author.

E-mail address: u9515915@nkfust.edu.tw

applied to investigating the transformation and transportation of air pollutants in the atmosphere. The effects of weather conditions on air pollutant concentrations are particularly interesting, which can be analyzed on the basis of the simulated results from various air quality and/or meteorological models, such as CALGRID (Yamartino *et al.*, 1992), MM5 (Grell *et al.*, 1994), CMAQ (Pai *et al.*, 2000; Wang *et al.*, 2017), MODEL3 (Zheng *et al.*, 2013), AERMOD (Kumar *et al.*, 2017), and CAM_X. In these studies, air quality and meteorological models are typically applied separately first and then together for comprehensively analyzing both fluid fields and air pollutant concentrations. However, extra efforts are usually required for combining these models, and meanwhile, some errors often happen. On the other hand, the Weather Research and Forecasting/Chemistry (WRF-Chem) model, established by the US government and academic groups after 2011, was developed by combining the WRF model with atmospheric chemical reaction models (Guenther *et al.*, 1993; Borge *et al.*, 2008; Yang *et al.*, 2017). The WRF-Chem model can thus more comprehensively and conveniently model the transport phenomena of air pollutants in the atmosphere (Kumar *et al.*, 2012; Lo and Hung, 2012). Thus, the WRF-Chem was applied in this research.

Taiwan is a small island but with a complex geography. The mountains with heights up to 4000 m are located along the Taiwan Island, causing both macro-meteorological conditions arising from the regional climate and micro-meteorological conditions resulting from high mountains affecting the flow patterns of air streams around and within Taiwan. Accordingly, a transboundary PMs-induced haze case occurring January 17–19, 2014, was investigated in this study. The phenomena for forming high-concentrated PMs, PM_{2.5} and PM₁₀, in the ambient air above the Taiwan Strait and over the Taiwan Island were analyzed. Both meteorological conditions and air pollutant concentrations in the aforementioned ambient air were recorded for further analysis and simulation with the WRF-Chem model. The intrinsic mechanisms underlying the transboundary air pollutant-induced formation of high-concentrated PMs in ambient air were discussed in the study. These results can provide essential information for air quality management.

METHODOLOGY

WRF-Chem Model Operating and Parameters Setting

Starting from January 17, 2014, a strong continental cold high-pressure system originating in northern China blew down to Far East Asia. This cold high-pressure system affected Taiwan weather from the noon of January 17 (see Fig. 1) and considerably deteriorated the ambient air quality from the morning of January 18 till noon on January 19. In this study, the WRF-Chem model was used to simulate both PM₁₀ and PM_{2.5} concentrations in the ambient air of Taiwan during the period of January 17–19, 2014 (China Standard Time). In order to make the numerical model operate more stably and accurately, the period from January 15 00 Z till January 17 00 Z (about 48 hours) was set as a pre-integration stage for model calculation for more

accurately modeling the concentrations of PMs after January 17 00 Z. Table 1 summarizes the parameter settings for operating the WRF-Chem model (Guenther *et al.*, 1994; Kumar *et al.*, 2017). There were three nesting domains used in this study (illustrated in Fig. 2). The outermost domain (D1) has a horizontal grid of 45 × 45 and a grid spacing of 81 km, which covers Far East Asia with a domain center point at 25°N, 120°E. The domain 2 (D2), covering the area of southeastern China including Taiwan, has a horizontal grid of 40 × 40 and a grid spacing of 27 km. The domain 3 (D3), designed to cover the whole Taiwan Island, has a horizontal grid of 47 × 59 and a grid spacing of 9 km (Table 1).

In addition, several data systems were applied for conducting the WRF-Chem model. For instance, both initial meteorological fields and boundary conditions were adopted from NCEP FNL Operational Global Analysis Data with 1° × 1°-resolution-degree grids for every 6 hours. Anthropogenic air pollutant emissions were estimated from the Regional Emission Inventory in Asia (REAS2007) and Taiwan Emission Database v 9.0 (TEDS 9.0) which included stationary, mobile, point, area, line, and natural sources (Taiwan EPA, 2016). Natural emissions of gases and aerosols were based on online calculations of MEGAN (version 2) (Guenther *et al.*, 2006; Yang *et al.*, 2018). Gas-phase chemical reactions for PMs in the model were calculated by the mechanisms proposed by Statewide Air Pollution Research Center (SAPRC-99) (Carter, 2000). Finally, photolysis schemes reported by Madronich Fast Troposphere Ultraviolet Visible (F-TUV) were used for photolytic rate calculation in this study (Tie *et al.*, 2003).

Besides, several configurations provided by WRF-Chem were applied in this study, which included GODDARD shortwaves schemes (Chou *et al.*, 1998), RRTMG longwave radiation schemes (Clough *et al.*, 2005; Lacono *et al.*, 2008), and Yonsei University (YSU) planetary boundary layer (PBL) schemes (Hong and Noh, 2006). The YSU scheme could accurately simulate deeper vertical mixing in buoyancy-driven PBLs with shallower mixing in strong-wind regimes compared to medium-range forecast (MRF) model schemes (Hong and Lim, 2006). The meteorological data from Taiwan EPA's monitoring stations were also introduced into the WRF-Chem through FDDA (four-dimensional data assimilation) for model simulating (Kumar *et al.*, 2017; Yang *et al.*, 2017).

Air Pollutant Emission Inventories and Air Quality Data

Air pollutant inventories for Asia, the regional emission inventory in Asia (REAS) Version 1.1) from 2014, were collected for this study. REAS is an air pollutant inventory that integrates historical, present, and possible future emissions in Asia on the basis of a consistent methodology. The target area for this study is from south to east Asia ranging from 50°N to 10°S in latitude and from 60°E to 150°E in longitude (Kurokawa *et al.*, 2013; Saikawa *et al.*, 2017).

Additionally, hourly concentrations of PMs were collected from ambient air quality monitoring stations located within Taiwan and on offshore islands established by the Taiwan Environmental Protection Agency. Data on the PM

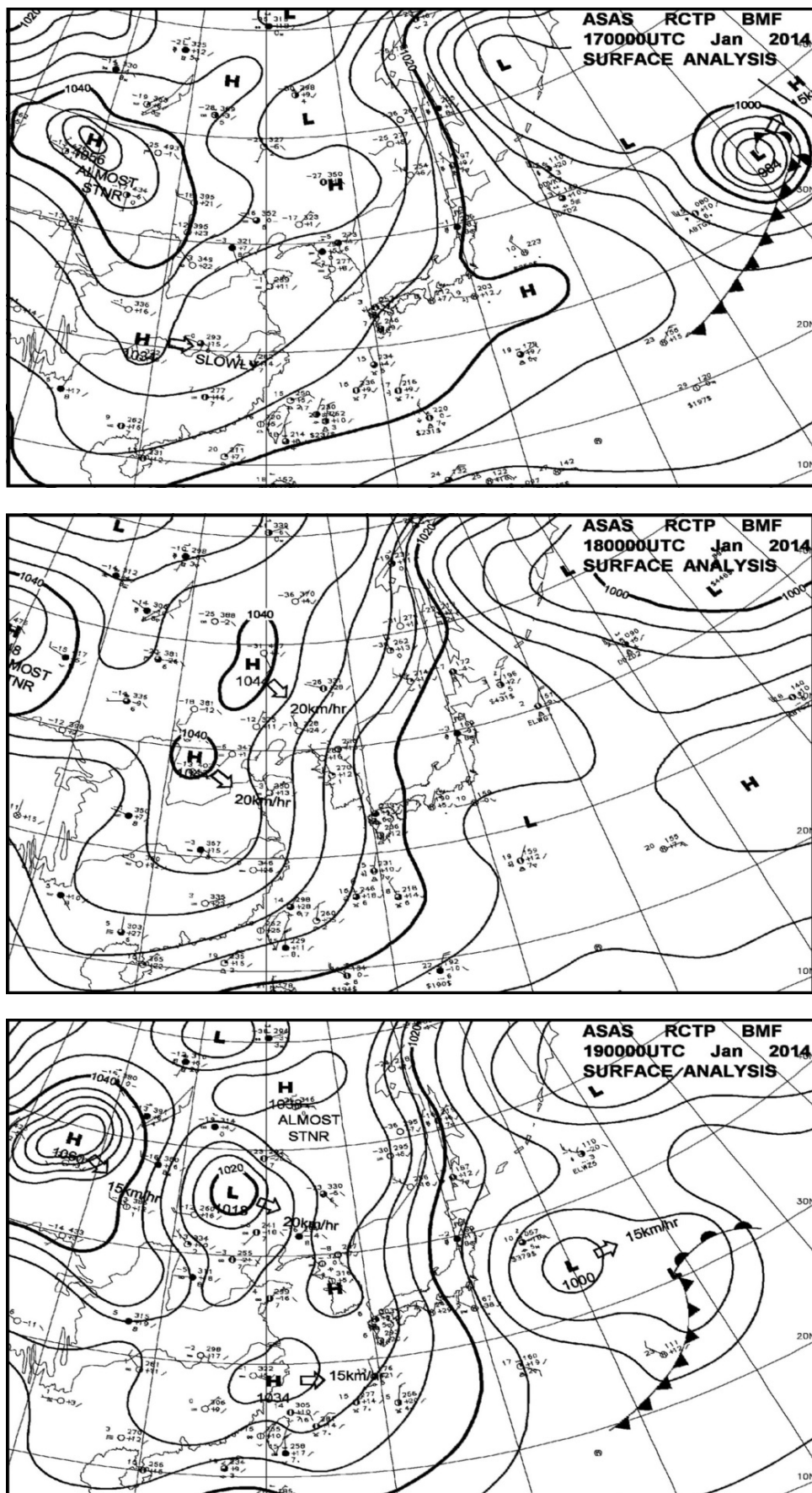
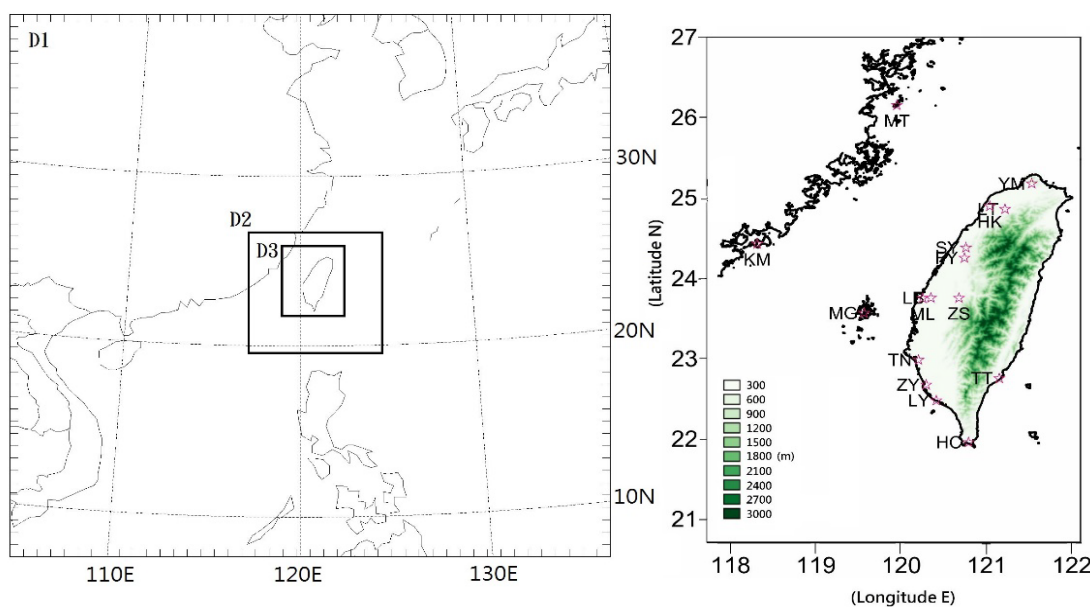


Fig. 1. Surface weather charts for Jan. 17, 18 and19, 2014 (data from Taiwan CWB).

Table 1. WRF/Chem model domain setting and simulation configurations.

Domain setting	D1	D2	D3
Domain		East Asia	Taiwan area
Domain point (x,y)	45,45	40,40	47,59
Horizontal resolution	81-km	27-km	9-km
Vertical resolution	27 layers from surface to 100 hpa (~16 km)		
Physical and chemical processes			
Microphysics	Morrison (Chen and Dudhia, 2001; Morrison <i>et al.</i> , 2009; Yang <i>et al.</i> , 2017)		
Cumulus	Grell 3D ensemble (domain D1 and D2), none for D3 (Grell and Freitas, 2014)		
Planetary Boundary Layer (PBL)	Yonsei University Scheme (YSU) (Hong and Lim, 2006 ; Hong and Noh, 2006)		
Anthropogenic emission	Regional Emission inventory in Asia (REAS2007); Taiwan Emission Database v9.0 (TEDS 9.0) (Lo and Hung, 2012)		
Biogenic emission	MEGAN 2;Taiwan Biogenic Emission Inventory System Version 2, TBEIS-2.0 (Guenther <i>et al.</i> , 2006)		
Photolysis	Madronich F-TUV (Tie <i>et al.</i> , 2003)		
Longwave radiation	Rapid and accurate Radiative Transfer Model for GCM (RRTMG) (Clough <i>et al.</i> , 2005; Lacono <i>et al.</i> , 2008)		
Shortwave radiation	GODDARD scheme (Chou <i>et al.</i> , 1998)		
Gas-phase chemistry	SAPRC-99 (Cater, 2000)		
Aerosol module	MADE/SORGAM and MADE/VBS (Grell <i>et al.</i> , 2005; Shrivastava <i>et al.</i> , 2011)		

**Fig. 2.** Modelling domain and terrain height for the WRF-Chem model.

concentrations were obtained from more than 80 ambient air quality monitoring stations. The daily peak concentrations of PM_{2.5} and PM₁₀ and the mass ratio of PM_{2.5} to PM₁₀, measured at 16 representative air quality monitoring stations, including the stations located on offshore islands (Matsu, Kinmen, and Penghu), in northern Taiwan (Yangming,

Longtan, Hukou, and Sanyi), in central Taiwan (Fengyuan, Chushan, and Lunbei), and in southern Taiwan (Tainan, Qiaotou, Linyuan, Hengchun, and Taitung), are summarized in Table 2 and depicted in Fig. 2. Among these 16 stations, 3 of them are on small islands in the Taiwan Strait, and the rest of them are in various locations of Taiwan Island.

Table 2. Locations of air quality monitoring stations and observed PM concentrations.

Location and GPS of Air quality station		Daily peak concentrations of PMs (ratio of PM _{2.5} to PM ₁₀)		
Location	GPS (Lat. Lon)	Jan. 17 th	Jan. 18 th	Jan. 19 th
<i>Stations on the islands on Taiwan Strait</i>				
Matsu (MT)	26°9'37.69" (N) 119°56'59.55" (E)	42/62 (0.68)	165/214 (0.77)	151/197 (0.77)
Kinmen (KM)	24°25'55.68" (N) 118°18'44.12" (E)	64/106 (0.60)	125/186 (0.67)	129/202 (0.64)
Magong (MG)	23°34'08.51" (N) 119°33'58.17" (E)	25/53 (0.47)	87/149 (0.58)	82/138 (0.59)
<i>Stations in northern Taiwan</i>				
Yangming (YM)	25°10'57.8" (N) 121°31'46.5" (E)	16/24 (0.67)	76/93 (0.82)	44/56 (0.79)
Longtan (LT)	24°51'49.93" (N) 121°12'58.86" (E)	28/58 (0.48)	103/159 (0.65)	58/97 (0.60)
Hukou (HK)	24°54'00.51" (N) 121°02'19.15" (E)	27/40 (0.68)	104/153 (0.68)	73/99 (0.74)
<i>Stations in middle-western Taiwan</i>				
Sanyi (SY)	24°22'58.59" (N) 120°45'31.80" (E)	35/55 (0.64)	101/165 (0.61)	71/109 (0.65)
Fengyuan (FY)	24°15'23.71" (N) 120°44'30.16" (E)	36/72 (0.50)	109/180 (0.61)	77/135 (0.57)
Zhushan (ZS)	23°45'23.00" (N) 120°40'38.30" (E)	52/99 (0.53)	105/218 (0.48)	100/138 (0.73)
Lunbei (LB)	23°45'27.17" (N) 120°20'55.47" (E)	57/109 (0.52)	138/680 (0.20)	105/173 (0.61)
Mailao (ML)	23°45'12.62" (N) 120°15'6.57" (E)	61/296 (0.21)	109/588 (0.19)	99/141 (0.70)
<i>Stations in southern Taiwan</i>				
Tainan (TN)	22°59'04.49" (N) 120°12'09.42" (E)	59/190 (0.31)	124/408 (0.30)	134/197 (0.68)
Qiaotou (QT)	22°45'27.02" (N) 120°18'20.48" (E)	49/164 (0.3)	103/331 (0.31)	121/219 (0.55)
Zouying (ZY)	22°40'29.5" (N) 120°17'34.5" (E)	55/157 (0.35)	125/300 (0.42)	152/218 (0.70)
Linyuan (LY)	22°28'46.2" (N) 120°24'42.3" (E)	64/90 (0.71)	95/182 (0.52)	100/133 (0.75)
Hengchun (HC)	21°57'29.05" (N) 120°47'20.14" (E)	16/31 (0.52)	53/90 (0.59)	43/77 (0.56)
<i>Stations in eastern Taiwan</i>				
Taitung (TT)	22°45'19.29" (N) 121°09'1.62" (E)	16/40 (0.40)	59/114 (0.52)	58/176 (0.33)

Modeling Results Confirming

Calculation root mean square errors (RMSE) for the simulated results by WRF-Chem were calculated and compared with observed data for confirming the accuracy of the modeling.

$$\text{RMSE} = \sqrt{\bar{(f - o)^2}} \quad (1)$$

where:

f: forecasts (simulated results),

o: observed values (observed results).

The bar above the squared differences is the mean (similar to \bar{x}). The same formula can be written with the following, slightly different notation (Barnston, 1992):

$$RMSE_{fo} = \left[\sum_{i=1}^N (Z_{fi} - Z_{oi})^2 N^{-1} \right]^{1/2} \quad (2)$$

where:

$(Z_{fi} - Z_{oi})^2$: differences, squared

N: sample size.

RESULTS AND DISCUSSION**Weather Systems**

Fig. 1 illustrates the major weather systems around Taiwan from January 17 till 19 in 2014. On the morning of January 17, 2014, strong and cold high pressure, a cold outburst formed in Mongolia ($40^{\circ}20'–50^{\circ}5'N$, $106^{\circ}–121^{\circ}40'E$),

moved eastward by following the direction from northern China to Shandong and Bohai Bay ($37^{\circ}07'–41^{\circ}N$, $117^{\circ}35'–121^{\circ}10'E$). After January 18, 2014, the strong cold northwest winds brought continental cold high pressure, traveled along East Asia, and turned into northeast winds after passing $30^{\circ}N$. The northeastern monsoon features a core cold high pressure system with a low relative humidity (< 55%). While moving down south to the areas near Taiwan and Fujian (east coast of China), the winds continued blowing southwards along the region between the Taiwan Strait and west coast of Taiwan (Fig. 1). However, the radiative cooling effect at night was strong enough to deteriorate the ambient air quality over Taiwan. In fact, surface atmosphere was stable and had high density (Streets *et al.*, 2003). Furthermore, because the Taiwan Strait becomes narrow around the middle of Taiwan, whereas it stretches to the south of the latitudinal positions, the divergence of air currents resulting from the Venturi effect weakens the strong northeastern monsoon over the Strait and redirects the wind to blow northwestwardly.

Both northern and central Taiwan, including offshore islands (Kinmen, Matsu, and Penghu), were within the reach of the northeastern monsoon caused by the continental high pressure system, but southern and eastern Taiwan were under the southwest edge of the high pressure system. The wind direction began to turn weak eastwards from the northeast gradually, causing atmospheric conditions unfavorable to air pollutant dispersion in the ambient air of southern Taiwan. When the northeast monsoon reached the south end of the Central Mountain Range, it might have gone over Hengchun Peninsula, characterizing lower terrain followed by blowing northeastwardly and moving into the waters to the southwest of Hengchun under the geostrophic effect. Two air currents converged offshore while the wake area formed along the coast with a mild horizontal wind speed.

PM Concentration Variation

For this study, data on the PM concentrations were obtained from more than 80 ambient air quality monitoring stations established by the Taiwan Environmental Protection Agency (Taiwan EPA). The daily peak concentrations of $PM_{2.5}$ and PM_{10} and the mass ratio of $PM_{2.5}$ to PM_{10} for the 16 represented ambient air quality monitoring stations (Fig. 2) are summarized in Table 2. The ambient $PM_{2.5}$ and PM_{10} concentrations for certain stations increased to unusually high levels, up to 152 and $680 \mu g m^{-3}$, respectively, while the continental cold high-pressure system approached Taiwan region. The concentrations were much higher than the air quality standards proposed by the Taiwan EPA, $35 \mu g m^{-3}$ for $PM_{2.5}$ and $65 \mu g m^{-3}$ for PM_{10} .

Moreover, the $PM_{2.5}$ to PM_{10} ratios during the investigation period peaked at 0.8 (besides at certain Lunbei and Mailao stations), which was relatively higher than those usual at this time of the year, 0.4–0.6. In particular, the $PM_{2.5}$ to PM_{10} ratios recorded at the offshore stations in Matsu and Kinmen Islands located near China. The ratios of $PM_{2.5}$ to PM_{10} in northern Taiwan were relatively higher (0.6–0.8) throughout the investigated period. This kind of high ratio situation indicated that more $PM_{2.5}$ might be brought in

Taiwan than PM_{10} , although both concentrations of them increased at the same time. Maybe the ratio of $PM_{2.5}$ to PM_{10} can be applied as an indicator for the invasion of transboundary PMs if more case studies can be collected and analyzed.

By contrast, for this case study, the ratio in both the mid-western and southern regions of Taiwan was initially low and then increased to high levels. All of these observations indicated that transboundary air pollutants or precursors for secondary air pollutants from China firstly affected Matsu Island and then influenced central Taiwan before finally affecting southern Taiwan. Among the 16 represented stations (Table 2), the stations at Lunbei and Mailao reported the lowest $PM_{2.5}$ to PM_{10} ratios, which was caused by the fact of the PM_{10} concentrations at these stations keeping high from January 17 till 18. This kind of high-concentrated PM_{10} resulted from the formation of mild-typhoon like winds in mid-western Taiwan (speed $> 15 m s^{-1}$). This kind of strong wind was induced by the approaching cold front lifted fugitive dust, including unpaved road dust and river sand, into the atmosphere, causing the PM_{10} concentration at the Lunbei station to reach $680 \mu g m^{-3}$. Similar phenomena were also observed at the other stations located in central Taiwan ($23^{\circ}50'–24^{\circ}25'N$, $120^{\circ}15'–120^{\circ}45'E$).

Figs. 3(a)–3(d) illustrates the temporal variation of measured PM concentrations and relative humidity variations during the period of January 17–19, 2014, at four representative air quality monitoring stations, namely, the Matsu, Longtan, Mailao, and Zouying stations. The Matsu station is located on Nangan Island, which is a small island located less than 10 km from Mainland China; its ambient air quality is thus easily affected by the air pollutants from the southeastern coast of China. Northern, northwestern, and northeastern winds may all transport airborne pollutants to the Matsu station. The other three stations are located in the northern, middle, and southern regions of Taiwan, respectively, and thus are representative of the ambient air quality in different places of Taiwan.

Figs. 3(a)–3(b) shows high PM concentrations in the ambient air across Taiwan, which was mainly contributed by the transboundary airborne PMs transported with the movement of a cold high-pressure system from the northwest to the southeast. Considerably high PM concentrations were reported during the 30th till 66th hour of the investigated period. Matsu achieved its peak concentration first, followed by Mailao, Longtan, and Zouying (Figs. 3(a) and 3(b)). Among these four stations, Matsu had the highest $PM_{2.5}$ concentration, $165 \mu g m^{-3}$, and Mailao had the highest PM_{10} concentration, $588 \mu g m^{-3}$. These peak PM concentrations occurred at approximately the 38th–40th hour when atmospheric humidity was less than 50% (Fig. 3(c)). Such poor air quality was caused by the transboundary air pollutants and local air pollutants. Fig. 4 illustrates the backward trajectories from the NOAA ARL Hybrid single-particle Lagrangian integrated trajectory simulation for both the Matsu and Kaohsiung stations, verifying the extent to which long-range transportation contributes to air pollutant concentrations. With January 21, 2014, as the base, the back trajectory analysis covered Matsu ($26^{\circ}09'37.69''N$,

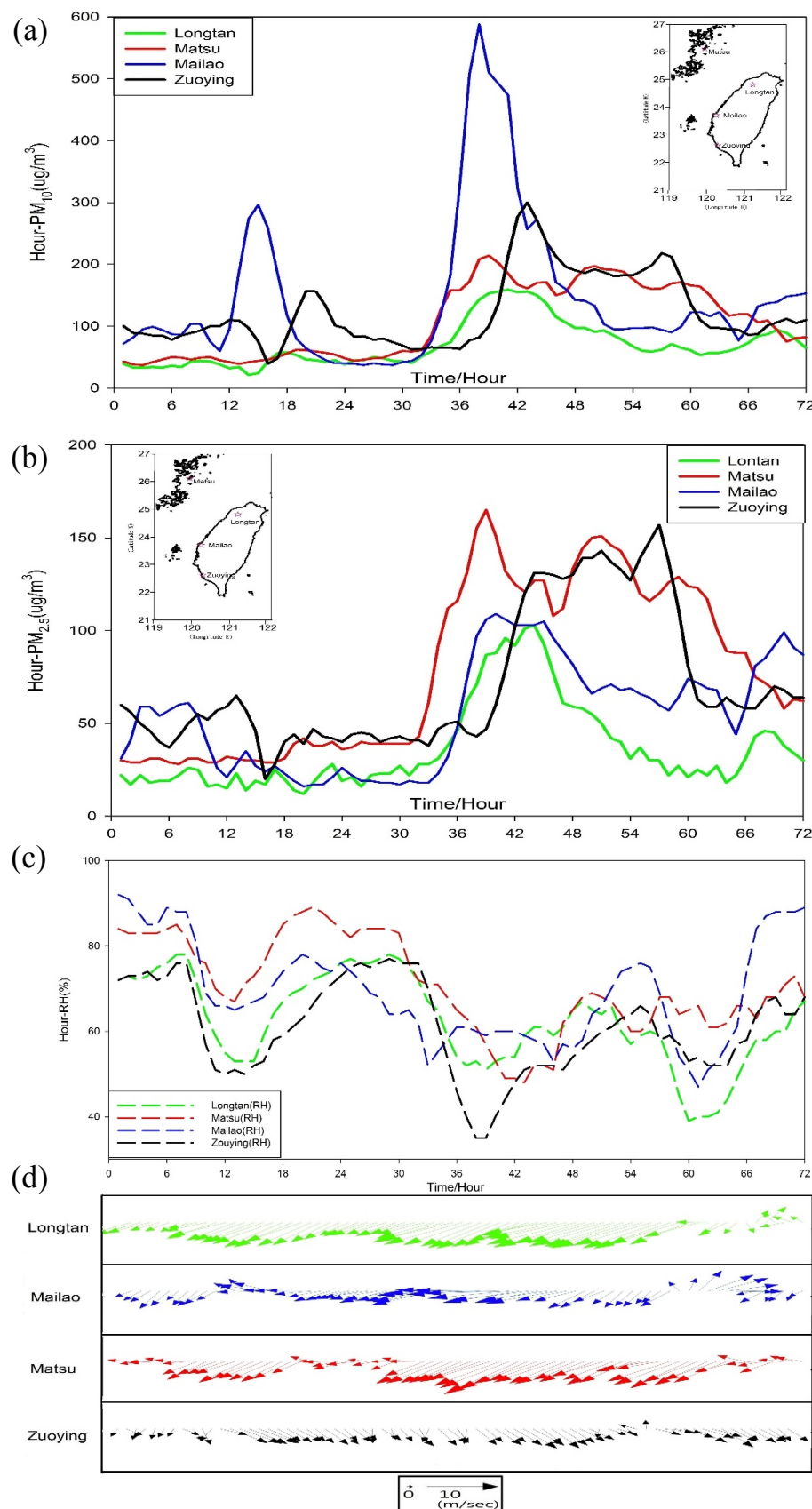


Fig. 3. (a)–(d) Observed PM concentrations of four represented ambient air quality monitoring stations (Matsu, Longtan, Mailao, Zouying) from Jan. 17 to 19, 2014. (Transboundary air pollutants arrived in Taiwan in the afternoon of Jan. 18, 2014).

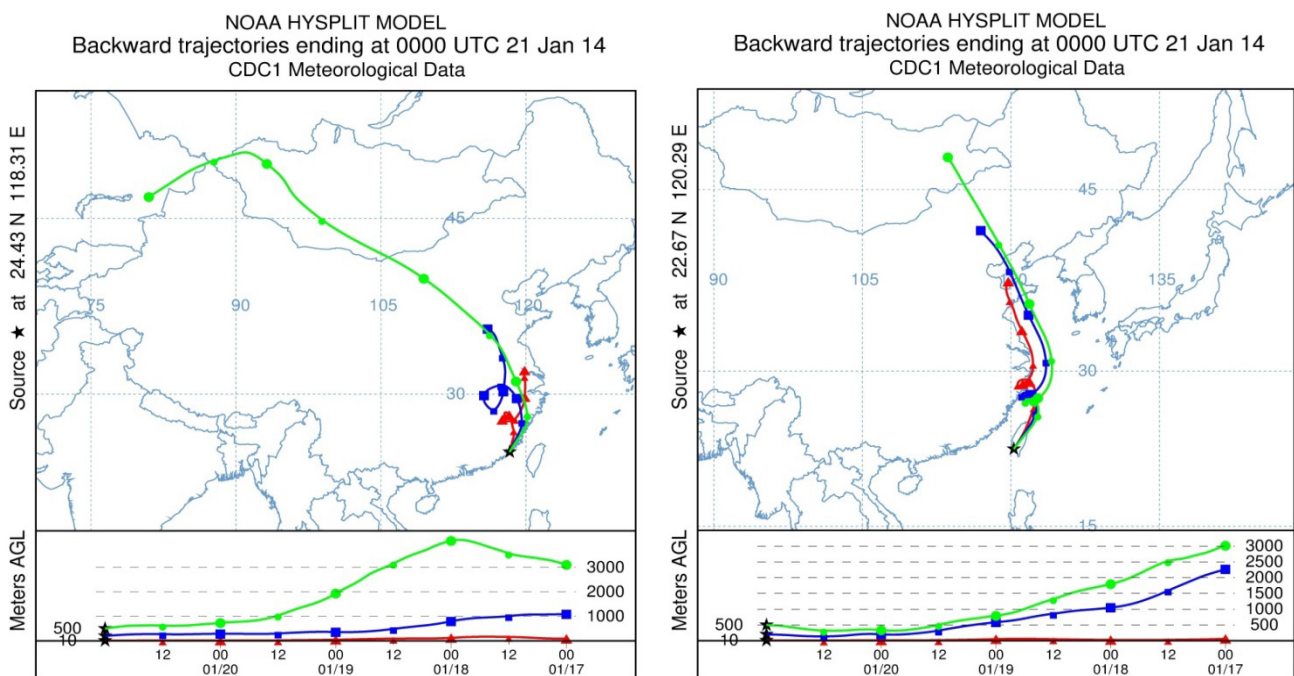


Fig. 4. Backward trajectories calculated from HYSPLIT, starting from 00UTC, Jan. 21st, 2014 backward for 96 hours at Kimen and Kaohsiung. (At 10, 20, 500 m above ground level (AGL)).

119°56'59.55"E) and Kaohsiung (22°38'N, 120°17'E) at heights of 10 m, 20 m, and 500 m for 96 hours. The continental cold air masses were shown to have originated in Mongolia and traveled southward through Beijing and Hebei before moving seaward to the southeast, affecting Taiwan (Fig. 4), thus confirming the transport of air pollutants from China to Taiwan.

The continental cold air masses transported air pollutants from China to Kimen and then to Taiwan, which moved through Beijing (39°26'–41°03'N, 115°25'–117°30'E), Tianjin (38°34'–40°15'N, 116°43'–118°19'E) and Heifei (30°57'–32°32'N, 116°41'–117°58'E). Checking historic air quality index data in China (<https://www.zq12369.com/environment.php>), the AQI index and PM concentrations increased from January 15. The AQI index ranged from 310 to 400 $\mu\text{g m}^{-3}$. The PM₁₀ concentrations were higher than 350 $\mu\text{g m}^{-3}$, and the PM_{2.5} concentrations were higher than 270–350 $\mu\text{g m}^{-3}$ at these three stations (Fig. 5).

In addition, as shown in Figs. 3(a)–(b), PM concentrations in the ambient air of East Asia rapidly increased to high levels after the morning of January 18 while the cold high-pressure system from China began to disperse southward. The high-pressure system contributed to a substantial increase in PM concentrations along the coast of East China, which was already completely enveloped in haze. The PM_{2.5} concentration in Matsu in the afternoon of January 18 was 165 $\mu\text{g m}^{-3}$ and peaked to 125 and 87 $\mu\text{g m}^{-3}$ at Kinmen and Magong, respectively, in the evening of January 18. Meanwhile, the PM₁₀ concentrations for the offshore stations were as high as 214 $\mu\text{g m}^{-3}$. During the period of January 17–19, the ambient air over most of Taiwan, particularly mid-western Taiwan, also had very high PM concentrations. The PM_{2.5} and PM₁₀ concentrations at the Lunbei station in

mid-western Taiwan, for example, were 138 and 680 $\mu\text{g m}^{-3}$, respectively, which were 4–10 times higher than the Taiwan EPA ambient air quality standards.

This severe haze case is a typical air pollution case caused by transboundary air pollutants. The PM concentrations increased from January 18 09:00. Before 14:00 on the same day, the PM_{2.5} concentrations were 104, 138, 125, and 59 $\mu\text{g m}^{-3}$ in northern, mid-western, southern, and eastern Taiwan, respectively. The PM₁₀ concentration in these regions was as high as 159, 680, 408, and 114 $\mu\text{g m}^{-3}$. Western Taiwan, particularly the mid-western and southern regions, had overwhelmingly high PM concentration conditions. The concentration of fine PM was about 10-fold higher than its normal concentration.

Following the early morning of January 19, both PM_{2.5} and PM₁₀ concentrations in northern and central Taiwan began to decrease, but those overseas (e.g., Matsu) and the southern Taiwan stations (e.g., Zuoying) maintained high PM conditions until the midnight of January 19. Matsu's high PM concentration was attributed to its nearness to China. As shown in Fig. 3(d), during the period of January 17–19, strong northeast winds continuously brought air pollutants to Matsu, thus deteriorating its ambient air quality dramatically. After January 19, although the cold high-pressure system had weakened, the air quality in southeastern coastal regions of China was still poor, and air pollutants from China continuously affected Matsu.

The PM concentration in Zuoying peaked after it peaked in Matsu and Mailao. Atmospheric humidity in Zuoying was lower than at other stations, which might be a side effect of the atmospheric subsidence in southwestern Taiwan caused by the northeastern monsoon winds. Finally, the PM concentrations in northern Taiwan were still 2–3 times



Fig. 5. AQI index and Observed PM concentrations of three represented ambient air quality monitoring stations (Beijing, Tianjin, Hefei) from Jan. 10 to Jan. 18, 2014.

higher than usual. The northeastern monsoon continuously prevailed toward north Taiwan (Fig. 3(d)) during the investigated period, showing the typical flowing patterns of a cold high-pressure system and airborne pollutants travelling with the high-pressure winds.

Compared to other stations, the ambient air quality in Hengchun was less affected by the transboundary pollutants. Its PM concentration was about 1–2 folds higher than usual. The cold high-pressure system was considerably weakened by the time it arrived in southern Taiwan, a similar case to the Asian dust originating in China seldom reaching southern Taiwan (He *et al.*, 2015; Zhang *et al.*, 2015). The PM_{2.5} to PM₁₀ ratio in Hengchun station was the lowest among the investigated stations, further evidencing the weak influence of the transboundary air pollutants on southern Taiwan.

Simulated Results: Wind Fields and PM Concentrations

Fig. 6 depicts both observed (dotted lines) and the simulated (solid lines) PM concentrations at four representative ambient air quality monitoring stations during the period of January 17–19, 2014, at a resolution of 9 km. The simulated results agreed well (moderate correlation coefficients, except for certain cases of very high concentrations) with the measured PM_{2.5} and PM₁₀ concentrations (Zang *et al.*, 2016) (Fig. 7).

Both atmospheric wind fields and PM concentrations within the region covering Southeast Asia, including Taiwan, were simulated. First, the WRF-Chem model was simulated at two synoptic scale resolutions (81 and 27 km). Fig. 8 and Fig. 9, respectively, present the simulated spatial and temporal variations in PM₁₀ and PM_{2.5} concentrations and wind fields. The model was subsequently simulated at a

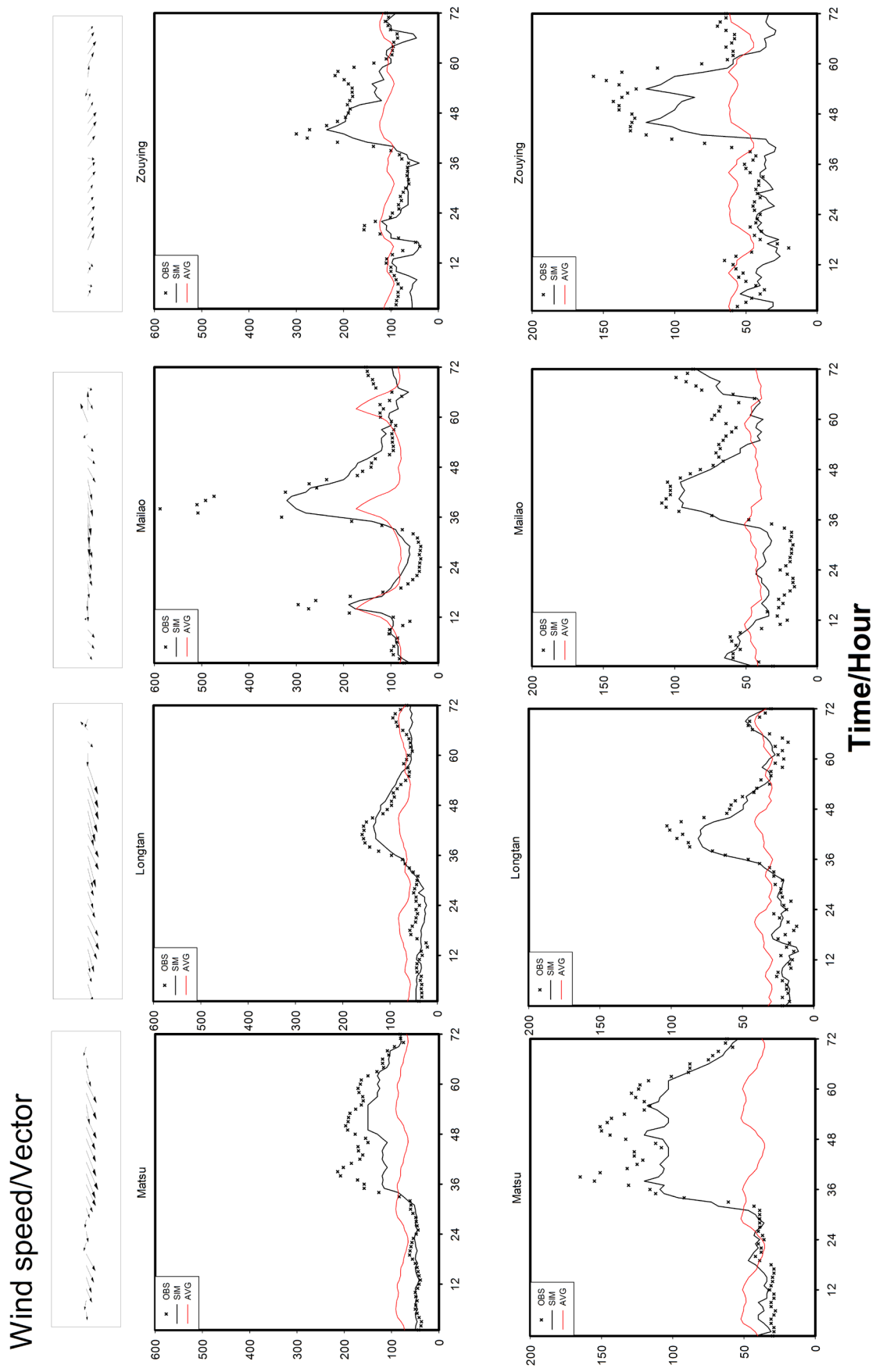


Fig. 6. Both observed and simulated PM_{10} and $\text{PM}_{2.5}$ concentration in the ambient air in Taiwan from Jan. 17 to 19, 2014 (Matsu, Longtan, Mailao, and Zouying stations).

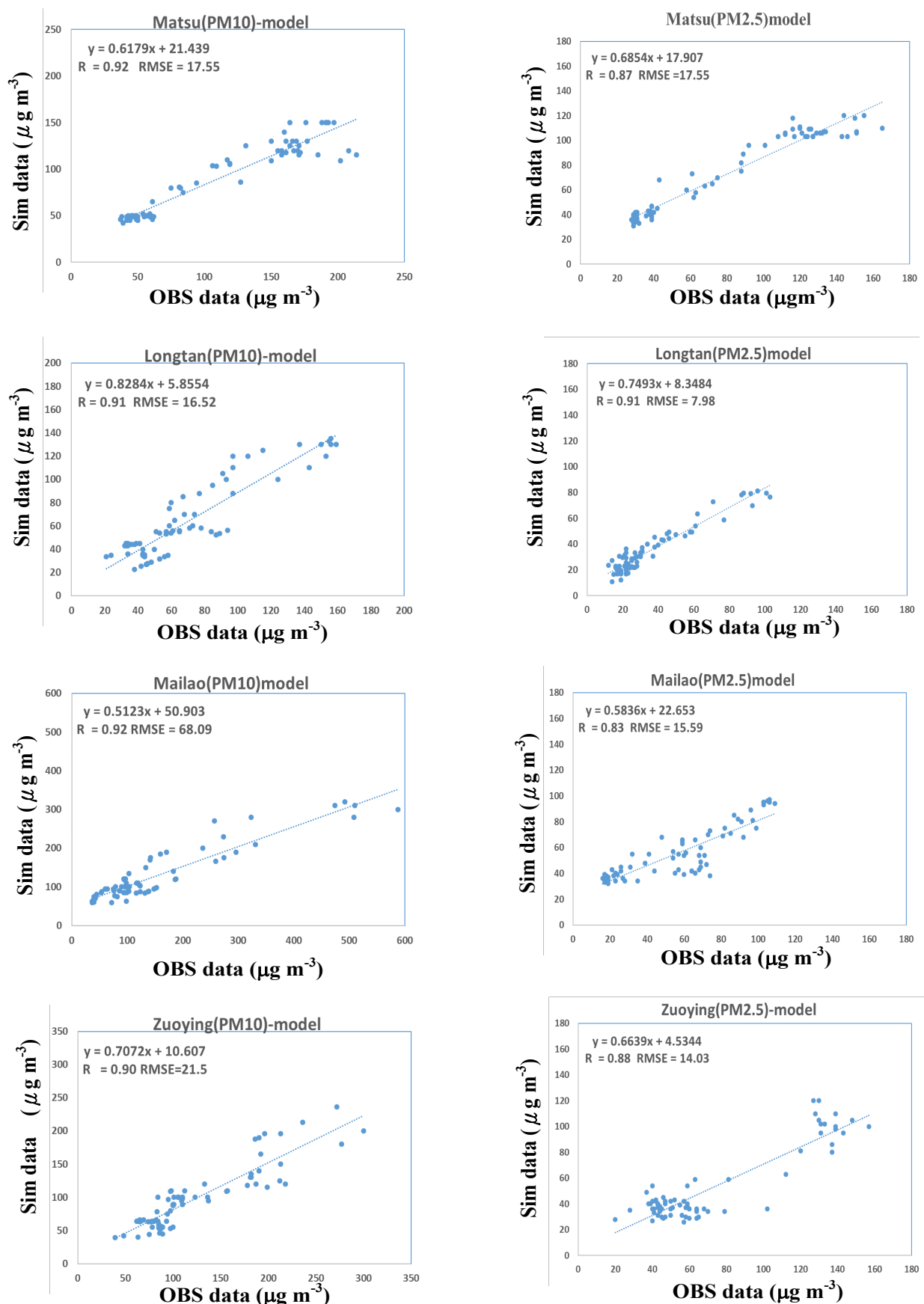


Fig. 7. Dispersion plots between observed (X-axis) and simulated PM concentrations (Y-axis) (Units in $\mu\text{g m}^{-3}$, PM_{10} is left column, $\text{PM}_{2.5}$ is right column).

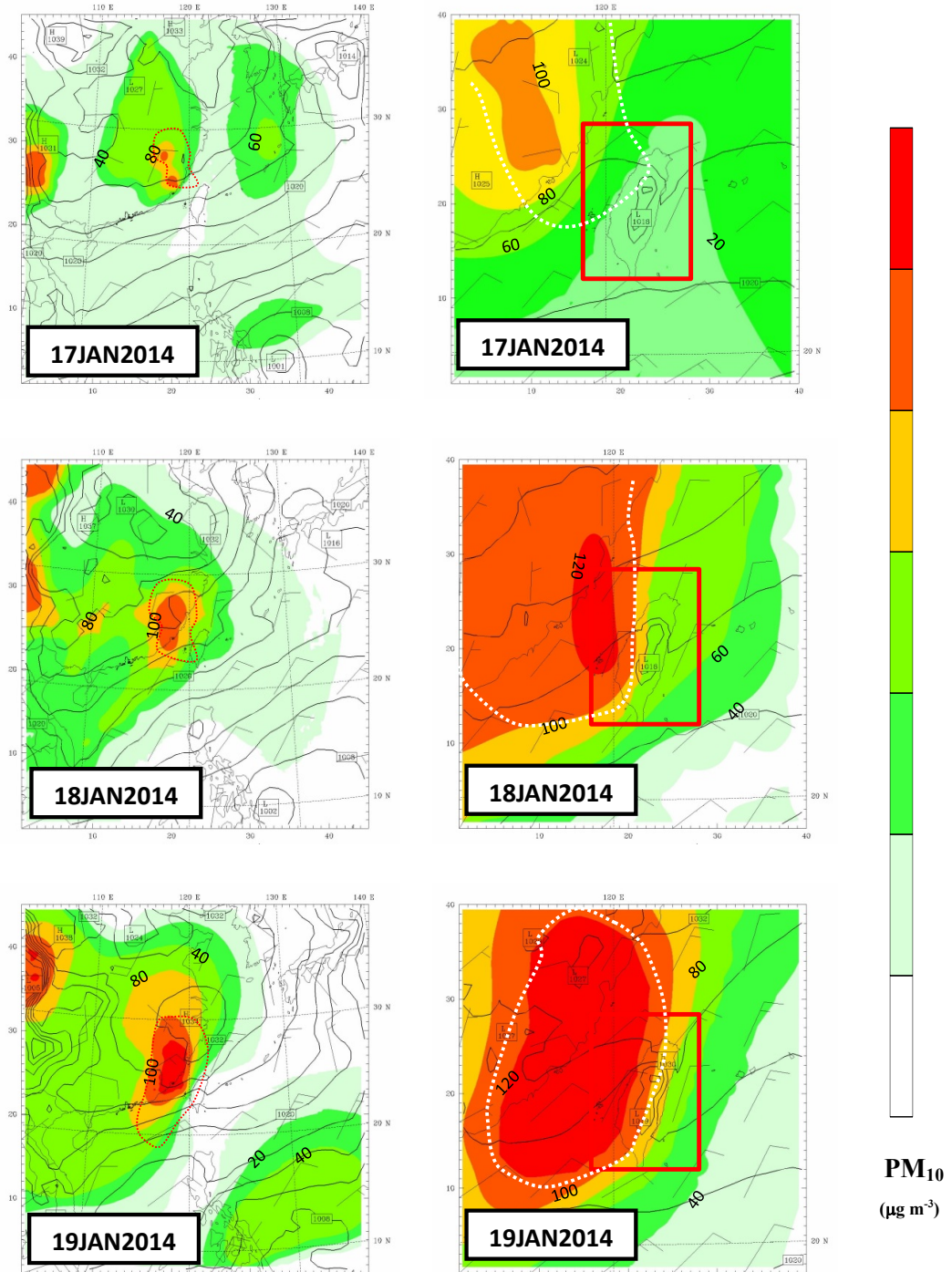


Fig. 8. Simulated surface PM₁₀ concentration contours and wind vectors in East Asia and Taiwan from Jan. 17 to 19, 2014 (Units: concentration in $\mu\text{g m}^{-3}$; wind vector full bar: 10 kt hr^{-1} , red (left column)/white (right column) dotted line: sulfate deposition flux $\geq 1 \mu\text{g m}^{-2} \text{ sec}^{-1}$; Left column is for D1-81 km, right column is D2-27 km).

higher resolution of 9 km for air pollutants and fluid fields on the Taiwan Island (Fig. 10). These simulations confirmed that the rapid deterioration of ambient air quality was mainly caused by the transboundary air pollutants from China. On January 17, a cold high-pressure system moved southeastward and transported air pollutants toward Taiwan. After passing 30°N, the high-pressure system moved farther southward along the region between the Taiwan Strait and

western Taiwan's Central Mountain Range. Meanwhile, PMs gradually accumulated in the ambient air of western Taiwan.

After the cold high-pressure system passed over Matsu, Kinmen, and Magong, the cold front entered mid-western Taiwan before moving over the rest of Taiwan. The PMs accompanying the cold front increased its concentration in the ambient air of most of Taiwan. But the cold front had

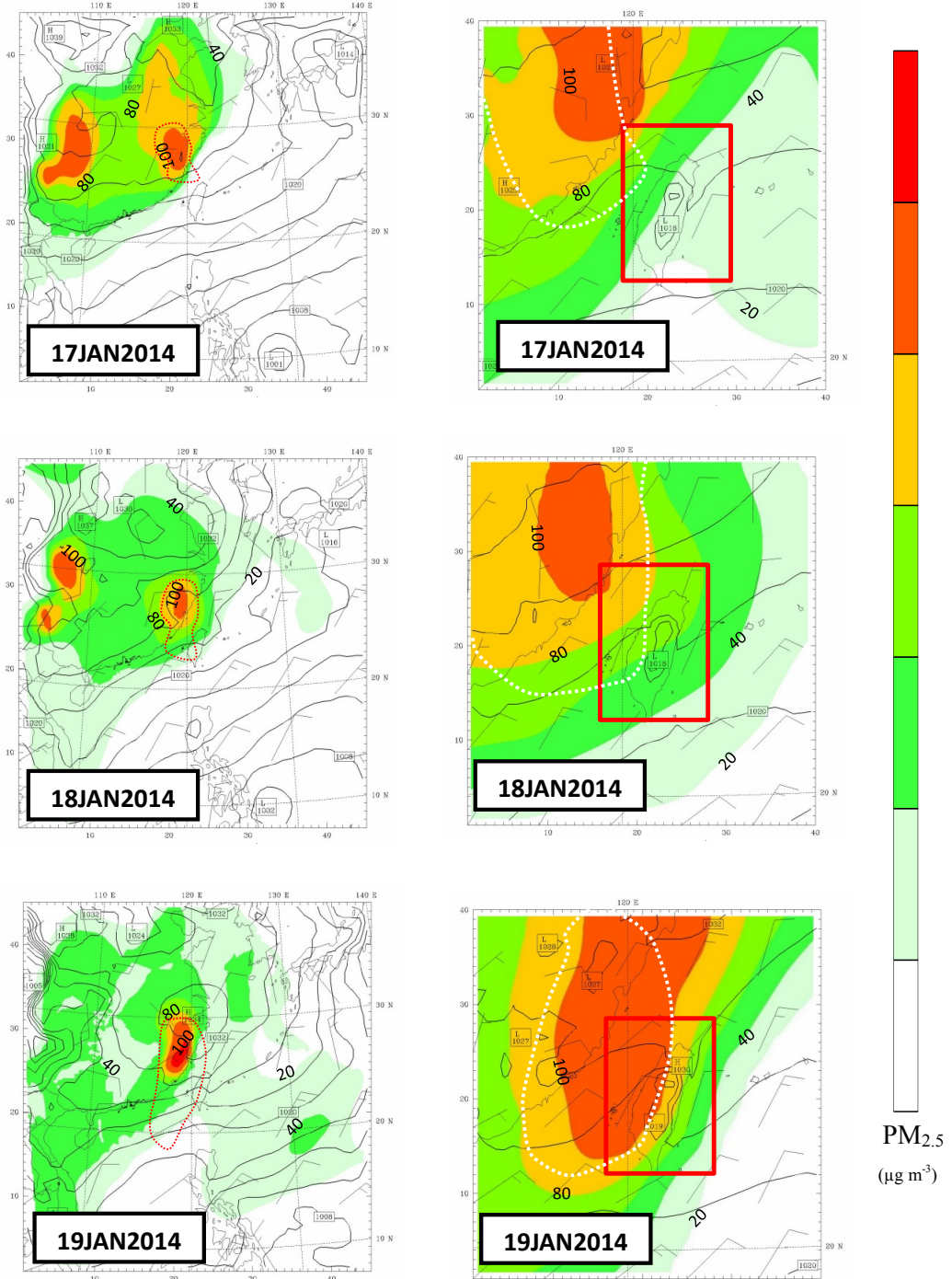


Fig. 9. Simulated surface PM_{2.5} concentration contours and wind vectors in East Asia and Taiwan from Jan. 17 to 19, 2014 (Units: concentration in $\mu\text{g m}^{-3}$; wind vector full bar: 10 kt hr^{-1} , red (left column)/white (right column) dotted line: sulfate deposition flux $\geq 1 \mu\text{g m}^{-2} \text{ sec}^{-1}$; Left column is for D1-81 km, right column is D2-27 km).

more influence on the western part of Taiwan than the eastern part of Taiwan (176 and $60 \mu\text{g m}^{-3}$, respectively) because the leeward side effects of the Central Mountain Range also contributed to increasing PM concentrations (Shrivastava *et al.*, 2011). The PM_{2.5} concentrations in southern Taiwan did not decrease until the morning of January 19, 2014, when the high pressure reflux was decreasing slowly.

Table 3 shows the MAE and RMSE values of ensemble WRF-CHEM simulations for the investigated air pollution. For the PM₁₀ case, the bias values indicated that the coupled models resulted in slightly positive biases of simulation except for 24 hours, which had a bias value of $9.21 \mu\text{g m}^{-3}$. The MAE and RMSE values of the three sequentially (24, 48, 72 hrs) did not change significantly, but the ensemble 72 hr simulation was associated with the lowest MAE value.

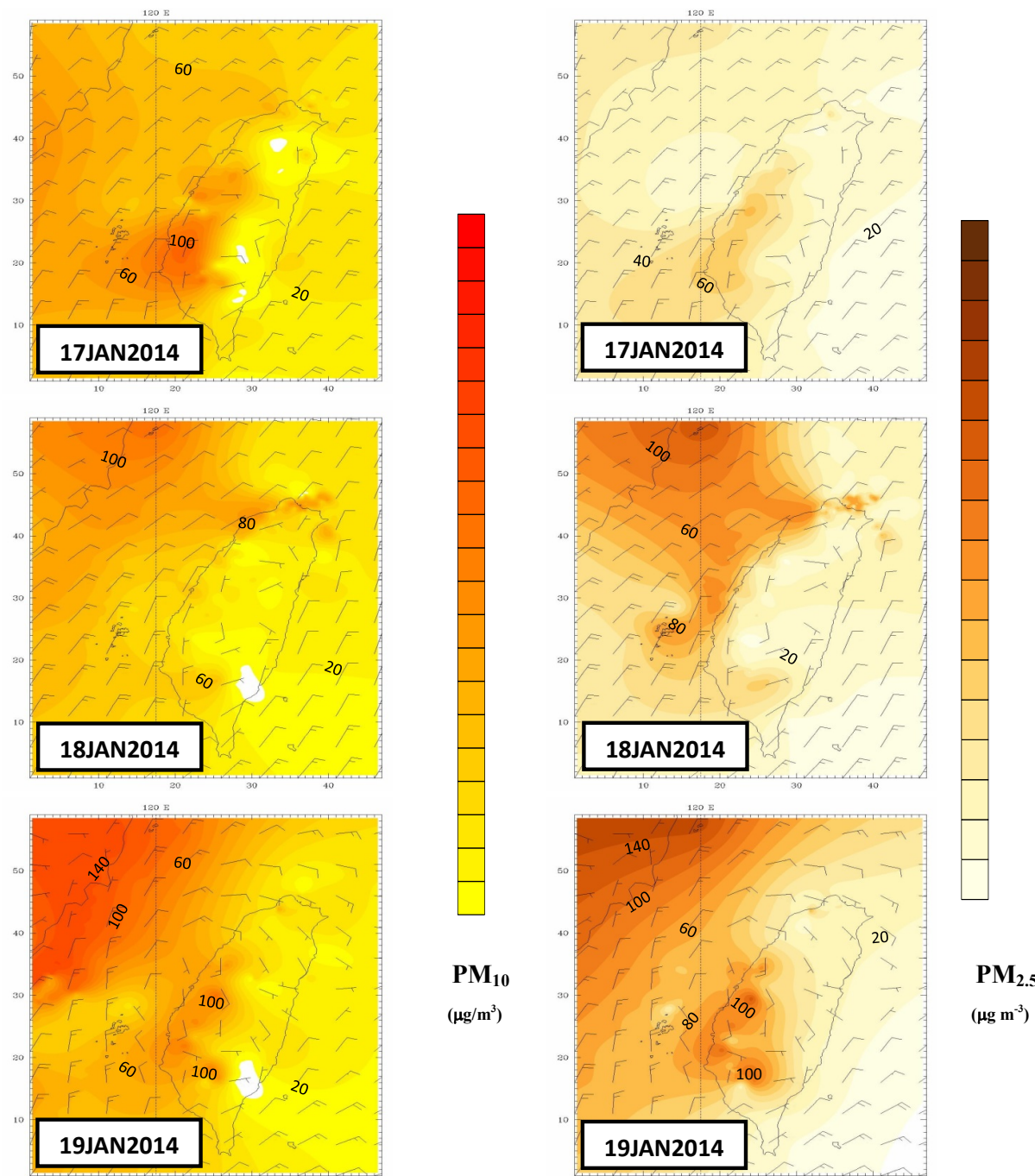


Fig. 10. Simulated PM₁₀ (left column) and PM_{2.5} (right column) concentrations ($\mu\text{g m}^{-3}$) and wind (bars) at 9 km-grid resolution on 04UTC Jan. 17–19, 2014.

Table 3. PMs statistical comparison (Bias, MAE, RMSE) between WRF/Chem simulated and observation.

Time	Jan. 17 th (24 hr)	Jan. 18 th (48 hr)	Jan. 19 th (72 hr)
PM ₁₀ ($\mu\text{g m}^{-3}$)			
Surface Bias	-9.21	-27.69	-17.31
Surface MAE	19.85	20.5	18.7
Surface RMSE	22.3	30.9	23.5
PM _{2.5} (μgm^{-3})			
Surface Bias	1.93	-7.42	-15.06
Surface MAE	8.2	9.1	13.1
Surface RMSE	10.3	10.4	13.5

The MAE values were 19.85, 20.5, and 18.7 $\mu\text{g m}^{-3}$ for the 24th, 48th, and 72th hr model simulations, respectively. In addition, the RMSE value of ensemble 24 hr simulations was reduced by 22.3, 30.9, and 23.5 $\mu\text{g m}^{-3}$ when compared to the 24th, 48th, and 72th hr modeling, respectively. Although the low concentration was within the range of the sampling error ($\leq 5\%$), the high concentration trend has more higher (5–8%). For the PM_{2.5}, the bias values indicated that the coupled models resulted in slightly positive biases (above observation data) in the simulation except for the 24th hr, which had a bias value of 1.93 $\mu\text{g m}^{-3}$. The MAE and RMSE value of the three sequentially (24th, 48th, 72th hr) did not change significantly, but the ensemble 24th hr simulation was associated with the lowest MAE value. The MAE values were 8.2, 9.1, and 13.1 $\mu\text{g m}^{-3}$ for the 24th, 48th, and 72th hr model simulations, respectively. Besides, the RMSE value of the ensemble 24th hour simulations was reduced by 10.3, 10.4, and 13.5 $\mu\text{g m}^{-3}$, respectively, compared to the 24th, 48th, and 72th modeling simulations. The PM₁₀ concentration has a large deviation value during the 24–48 hour period. The PM_{2.5} concentration has a large deviation value during the 48–72 hour period. Although the low concentration was within the range of the sampling error ($\leq 5\%$), the high concentration trend has more higher (5–10%).

Table 4 shows the forecast average errors at 4 stations over 3 days, which indicates a larger but still acceptable deviation in surface wind direction (up to 10 degrees for RMSE). For temperature, the average error value of 4 stations is small (meaning the forecast temperature is on the lower side). The best meteorological simulation appears in the pressure range from 1 to 24 hr. With the period changes of

48–72 hours, meteorological parameters the bias will gradually become larger for WRF model simulate.

Fig. 11 depicts the variation in PBL height for four representative air quality monitoring stations during the investigated period. Atmospheric PBL height can be an indicator for the height or threshold for a boundary layer and can be determined by vertical temperature changing in the atmosphere (Coniglio *et al.*, 2013; Yen *et al.*, 2013; Grell *et al.*, 2014; Li *et al.*, 2015; Wang *et al.*, 2017). The PBL height in the atmosphere is usually about 1000–2000 m during the daytime in winters, but it is often under 900 m or even lower in the night. For this case study, because the ground was heated by solar radiation during the daytime, the height of the boundary layer was about 1100 m. But in the night, with the decrease in solar radiation, the turbulence intensity in the boundary layer gradually decayed, and the PBL height decreased to as low as 410 m. On Jan. 18, 2014, the PBL height for both MT and LT was higher than 1200 m, but the height for the ML and ZY stations, stations in mid-western and southern Taiwan, respectively, was between 900 and 980 m. Consistently, PMs in ZY were higher than 125 $\mu\text{g m}^{-3}$ (PM_{2.5}) and 300 $\mu\text{g m}^{-3}$ (PM₁₀). High PM concentration is often observed under a low atmospheric PBL height (Fig. 11). As a matter of fact, most areas of Taiwan were under the effects of the high pressure system for this case study, causing the relatively low PBL height observed in most of Taiwan. Fig. 12 depicts the vertical profiles of both PM₁₀ and PM_{2.5}, showing the invasion of air pollutants from China to Taiwan with the movement of a high pressure system. During winters of Taiwan, the high pressure system often makes tropospheric

Table 4. Meteorological data statistical comparison (Bias, MAE, RMSE) between WRF/Chem simulated and observation.

Time	Jan. 17 th (24 h)	Jan. 18 th (48 h)	Jan. 19 th (72 h)
*** Temperature (°C) ***			
Surface Bias	−0.7842	−0.506	−0.7446
Surface MAE	2.589	2.342	2.647
Surface RMSE	4.186	2.9938	4.067
*** Dew point (°C) ***			
Surface Bias	−4.131	1.261	1.262
Surface MAE	4.979	2.707	2.735
Surface RMSE	5.847	4.028	4.008
*** Wind U Component (m s^{−1}) ***			
Surface Bias	−.8761	−1.992	−1.890
Surface MAE	1.897	2.910	2.979
Surface RMSE	2.470	3.886	3.909
*** Wind V Component (m s^{−1}) ***			
Surface Bias	−1.293	−1.788	−1.971
Surface MAE	2.408	3.104	3.297
Surface RMSE	3.110	4.066	4.250
*** Wind Direction (Deg) ***			
Surface Bias	4.462	12.297	12.317
Surface MAE	7.102	8.112	8.061
Surface RMSE	10.879	12.938	10.260
*** Wind Speed (m s^{−1}) ***			
Surface Bias	2.130	3.544	3.711
Surface MAE	2.493	3.700	3.868
Surface RMSE	3.168	4.734	4.887

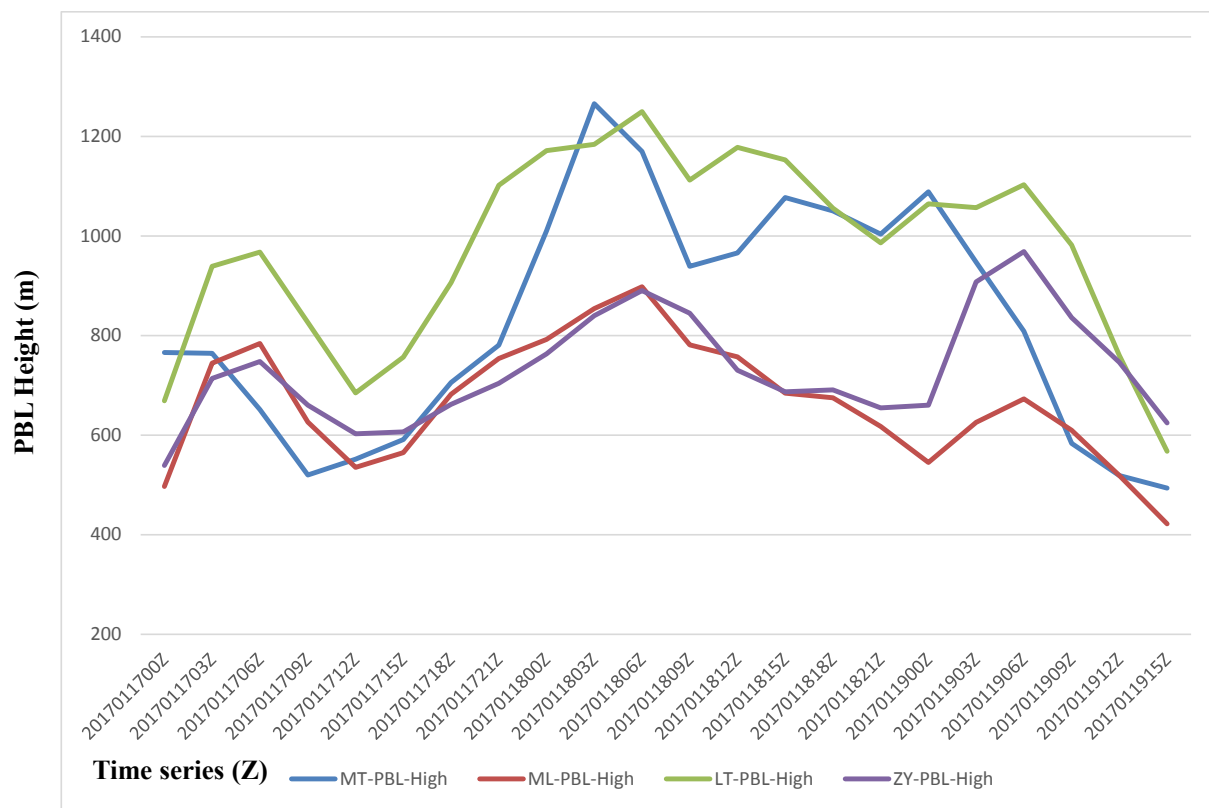


Fig. 11. Simulated PBL height (m) (Time series: X-axis PBL height: X-axis).

downwash and thus results in the formation of high air pollution cases.

On January 18, 2014, the Matsu station showed that the observed $\text{PM}_{2.5}$ concentration was $165 \mu\text{g m}^{-3}$ (Table. 2), while the simulated concentration was underestimated as about $110 \mu\text{g m}^{-3}$ (Fig. 12). There were some possible reasons for such underestimation, including inconsistencies in the emission inventory of PMs, especially for the emission sources in China, the special topographic surface conditions of the Taiwan Island unable to be reflected in the model, and the additional air pollutants (e.g., fugitive road dust generated by strong winds), which were not considered in the model (Chang *et al.*, 2015; Donkelaar *et al.*, 2015; Wang *et al.*, 2015; Cai *et al.*, 2016). Nevertheless, both the measured and simulated results clearly demonstrated that the long-range transported air pollutants from China substantially affected the ambient air quality in Taiwan from the early morning of January 18, 2014.

On the basis of the WRF-Chem simulations, the vertical atmospheric structures within the investigation area were analyzed with a simulated Skew-T log-P diagram for both Matsu and Lontan (Fig. 13). The dry cold air currents of the high-pressure systems started moving southward on January 17, resulting in a rapid overnight fall in temperature, the formation of a stable inversion layer, and the weakening of surface wind speeds. With the east wind approaching, the air pollutants accumulated and were trapped within the leeward side of the mountains of Taiwan. The vertical wind field also showed that the vertical atmosphere in Matsu (Fig. 13, left) generally featured downward motion and

temperature inversion during the period of January 17–19.

The simulated Skew-T log-P diagram of Mailao (left) and Zouying (right) illustrated in Fig. 14 shows that ground heat radiated strongly into the air at sunset on the windless and clear winter nights during the investigation period. Accordingly, ground and near-ground temperatures dropped rapidly. During the investigation period, the boundary layer in Zouying was at $< 900 \text{ hPa}$ (Fig. 14, right). However, the temperature in the higher atmospheric layers decreased relatively slowly. An inversion featuring high temperatures at high layers and low temperatures at low layers was formed. It was difficult for this inversion layer to disperse air pollutants vertically owing to insufficient sunlight and low temperatures during the day, which resulted in high ground-level air pollution throughout the day (Gao *et al.*, 2014; Chang *et al.*, 2015; Chen *et al.*, 2015).

CONCLUSIONS

The mechanisms underlying the increase in concentrations of PM during the period of January 17–19, 2014, over East Asia, including Taiwan, were investigated in this case study. Both PM_{10} and $\text{PM}_{2.5}$ peaked as high as 680 and $165 \mu\text{g m}^{-3}$, respectively, on January 18, 2014, mainly because of the transported transboundary air pollutants accompanying a cold high-pressure weather system. The WRF-Chem model was used to simulate and analyze the main mechanisms underlying the formation of high concentrations of PM in western Taiwan. Some important results of this study can be summarized as follows:

- (1) The cold high-pressure system featured low temperatures and dry and downward currents in the middle and higher atmospheric layers, which facilitated the long-range transport of air pollutants. The transported air pollutants significantly lowered the ambient air quality. In addition, the complex topography in western Taiwan led to the formation of wake areas and/or low inversion layers, consequently further deteriorating the ambient air quality.
- (2) The temperature inversion, which occurs frequently in winter, lowered the ambient air quality after nightfall.

The consistent mechanisms observed in this case study show that the rising indexes of air pollution were highly correlated with temperature inversion conditions.

- (3) The WRF-Chem model simulation confirmed that the air in western Taiwan was dry and moved downward for this case study, resulting in the formation of low inversion layers. The simulation was highly correlated with the measurements at stations upwind and downwind of the cold front, indicating that the pollution was contributed by the synergistic effects of the transported air pollutants and the topographic distribution mechanisms.

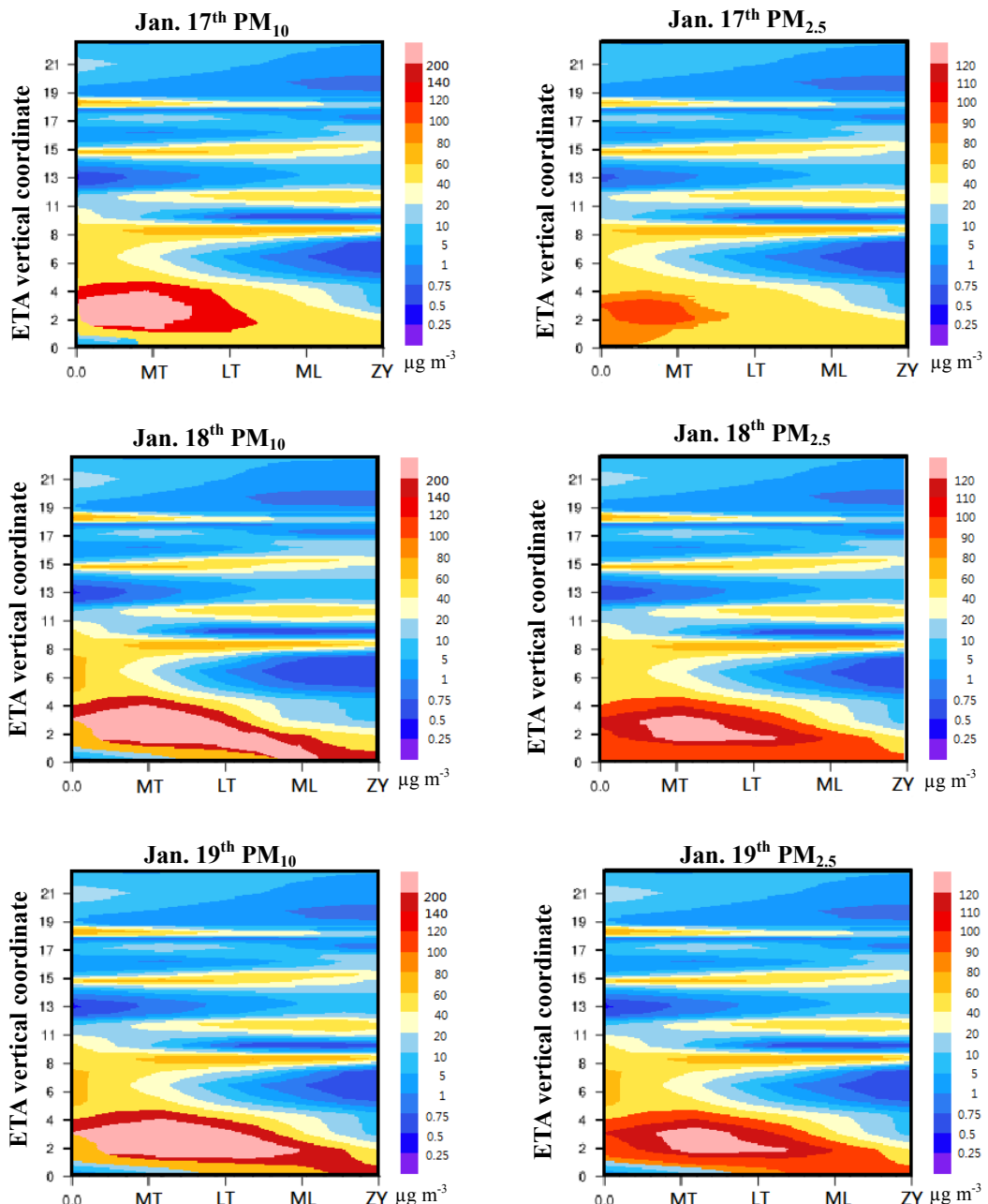


Fig. 12. WRF-Chem simulated vertical profile of PMs (PM_{10} $\text{PM}_{2.5}^{-1}$). (Station: X-axis, Model level (SURFACE (SFC): 0, 1000 hpa (near 180 m): 1, 975 hpa: 2, 950 hpa: 3, 925 hpa (near 800 m): 4, 900 hpa: 5, 850 (near 1500 m) hpa: 6, 800 hpa: 7, 750 hpa: 8, 700 hpa (near 3000 m): 9, 650 hpa: 10, 600 hpa: 11, 550 hpa: 12, 500 hpa (near 5500 m): 13, 450 hpa: 14, 400 hpa: 15, 350 hpa: 16, 300 hpa (near 9600 m): 17, 250 hpa: 18, 200 hpa: 19, 150 hpa: 20, 100 hpa (16500 m): 21: Y-axis).

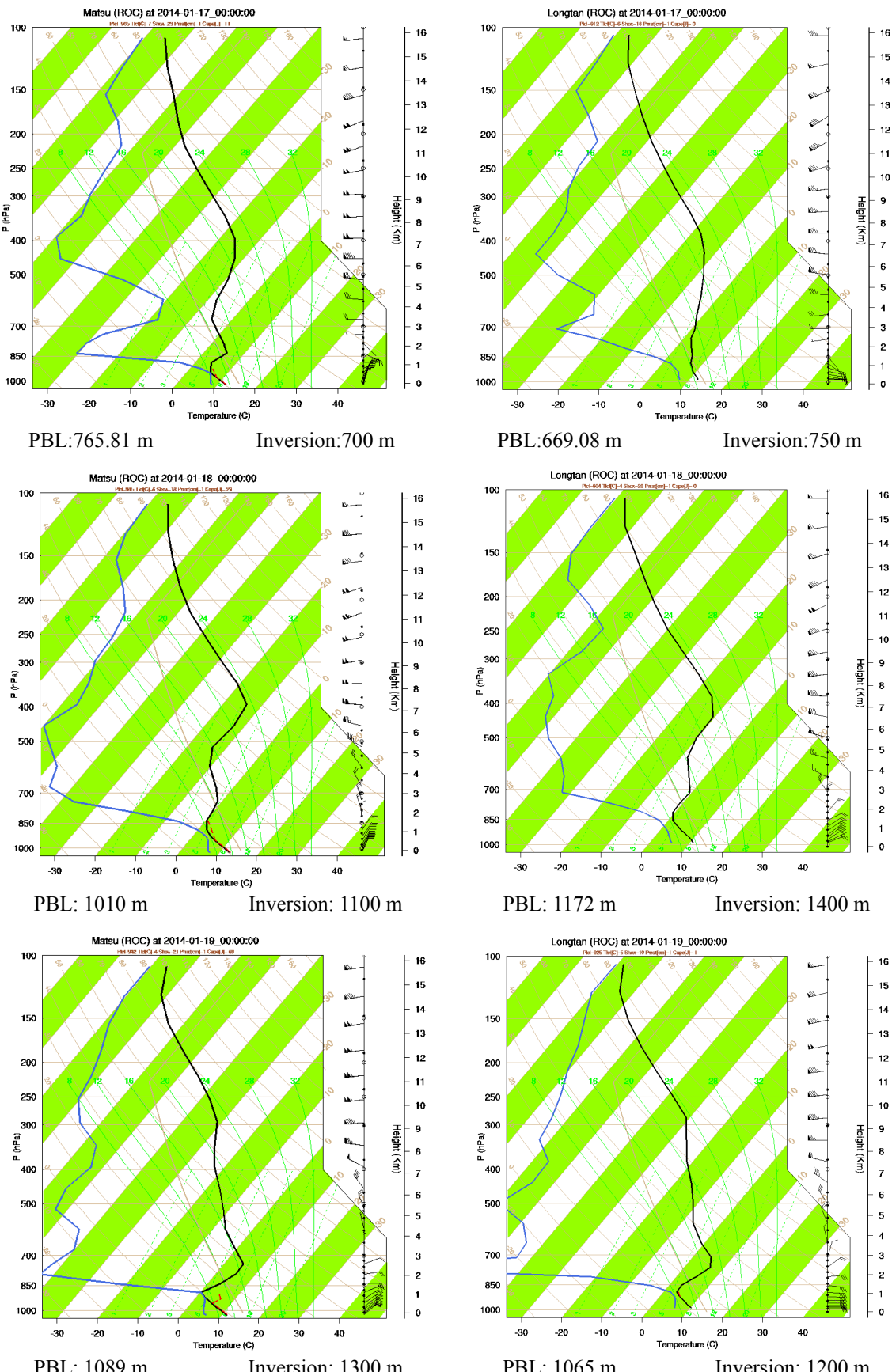


Fig. 13. Simulated skew-temperature diagram for Matsu and Longtan air quality monitoring stations (black line: temperature ($^{\circ}\text{C}$); gray line: dew-point temperature ($^{\circ}\text{C}$); wind vector full barb = 5 m s^{-1}).

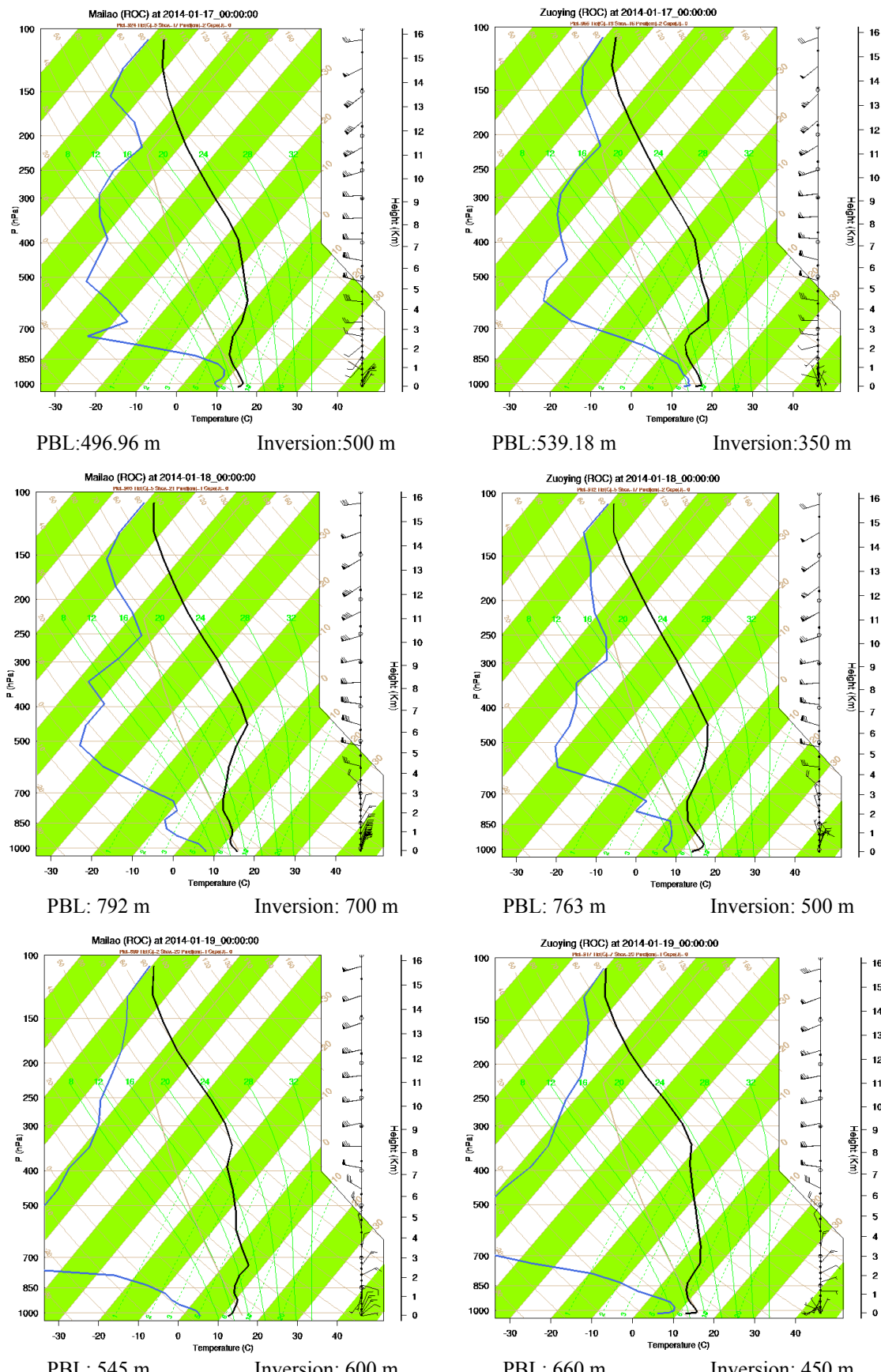


Fig. 14. Simulated skew-temperature diagram for Mailao and Zuoying air quality monitoring stations (black line: temperature ($^{\circ}\text{C}$); gray line: dew-point temperature ($^{\circ}\text{C}$); wind vector full barb = 5 m s^{-1}).

- (4) The model simulation demonstrated that the air pollutants were transported along the north-south direction in western Taiwan, whereas the cold and dry descending currents on the leeward side gradually moved southward. This led to the formation of high PM concentrations near the ground surface and to terrain downwash.

ACKNOWLEDGEMENTS

The authors would like to thank both the Ministry of Science and Technology, Taiwan, and the National Kaohsiung First University of Science and Technology for financially supporting this research under the contract numbers of MOST 105-2221-E-327 -003 -MY3 and MOST 105-EPA-F-008-002.

REFERENCES

- Borge, R., Alexandrov, V., José del Vas, J., Lumbreiras, J. and Rodríguez, E. (2008). A comprehensive sensitivity analysis of the WRF model for air quality applications over the Iberian Peninsula. *Atmos. Environ.* 42: 8560–8574.
- Cai, C., Zhang, X., Wang, K., Zhang, Y., Wang, L., Zhang, Q., Duan, F., He, K. and Yu, S.C. (2016). Incorporation of new particle formation and early growth treatments into WRF/Chem: Model improvement, evaluation, and impacts of anthropogenic aerosols over East Asia. *Atmos. Environ.* 124: 262–284.
- Carter, W.P.L. (2000). *Implementation of the SAPRC-99 chemical mechanism into the Models-3 framework*. Report to the United States Environmental Protection Agency.
- Chang, T.J., Chena, C.L., Tua, Y.L., Yeha, H.T. and Wu, Y.T. (2015). Evaluation of the climate change impact on wind resources in Taiwan Strait. *Energy Convers. Manage.* 95: 435–445.
- Chen, F. and Dudhia, J. (2001). Coupling an advanced land surface-hydrology model with the Penn State-NCAR MM5 modeling system. Part II: preliminary model validation. *Mon. Weather Rev.* 129: 587–604.
- Chen, J.L., Liu, H.H., Chuang, C.T. and Lu, H.J. (2015). The factors affecting stakeholders' acceptance of offshore wind farms along the western coast of Taiwan: Evidence from stakeholders' perceptions. *Ocean Coastal Manage.* 109: 40–50.
- Chou, M.D., Suarez, M.J., Ho, C.H., Yan, M.M.H. and Lee, K.T. (1998). Parameterizations for cloud overlapping and shortwave single-scattering properties for use in general circulation and cloud ensemble models. *J. Climate*. 11: 202–214.
- Clough, S.A., Shephard, M.W., Mlawer, E.J., Delamere, J.S., Iacono, M.J., Cady-Pereira K., Boukabara, S. and Brown, P.D. (2005). Atmospheric radiative transfer modeling: A summary of the AER codes. *J. Quant. Spectrosc. Radiat. Transfer* 91: 233–244.
- Coniglio, M.C., Correia, Jr. J., Marsh, P.T. and Kong, F. (2013). Verification of convection-allowing WRF Model forecasts of the planetary boundary layer using sounding observations. *Weather Forecasting* 28: 842–862.
- Donkelaar, A.V., Martin, R.V., Brauer, M. and Boys, B.L. (2015). Use of satellite observations for long-term exposure assessment of global concentrations of fine particulate matter. *Environ. Health Perspect.* 123: 135–143.
- Fang, Y., Naik, V., Horowitz, L.W. and Mauzerall, D.L. (2013). Air pollution and associated human mortality: the role of air pollutant emissions, climate change and methane concentration increases from the preindustrial period to present. *Atmos. Chem. Phys.* 13: 1377–1394.
- Fiore, A.M., Naik, V. and Spracklen, D.V. (2012). Global air quality and climate. *Chem. Soc. Rev.* 41: 6663–6683.
- Gao, Y., Zhao, C., Liu, X., Zhang, M. and Leung, L.R. (2014). WRF-Chem simulations of aerosols and anthropogenic aerosol radiative forcing in East Asia. *Atmos. Environ.* 92: 250–266.
- Grell, G.A., Dudhia, J. and Stauffer, D.R. (1994). A Description of the Fifth Generation Pennsylvania State/NCAR Mesoscale Meteorology Model (MM5). *NCAR Technical Note* NCAR/TN-398+STR.
- Grell, G.A., Peckham, S.E., Schmitz, R., McKeen, S.A., Frost, G., Skamarock, W.C. and Eder, B. (2005). Fully coupled online chemistry within the WRF model. *Atmos. Environ.* 39: 6957–6975.
- Grell, G.A. and Freitas, S.R. (2014). A scale and aerosol aware stochastic convective parameterization for weather and air quality modeling. *Atmos. Chem. Phys.* 14: 5233–5250.
- Guenther, A., Zimmerman, P. and Wildermuth, M. (1994). Natural volatile organic compound emission rate estimates for U.S. woodland landscapes. *Atmos. Environ.* 28: 1197–1210.
- Guenther, A.B., Zimmerman, P.R., Harley, P.C., Monson, R.K. and Fall, R. (1993). Isoprene and monoterpene emission rate variability: Model evaluations and sensitivity analyses. *J. Geophys. Res.* 98: 12609–12617.
- Guenther, A.B., Karl, T., Harley, P., Wiedinmyer, C., Palmer, P.I. and Geron, C. (2006). Estimates of global terrestrial isoprene emissions using MEGAN (Model of Emissions of Gases and Aerosols from Nature). *Atmos. Chem. Phys.* 6: 3181–3210.
- He, H., Tie, X., Zhang, Q., Liu, X., Gao, Q., Li, X. and Gao, Y. (2015). Analysis of the causes of heavy aerosol pollution in Beijing, China: A case study with the WRF-Chem model. *Particuology* 20: 32–40.
- Hong, S.Y. and Lim, J.O.J. (2006). The WRF single-moment 6-class microphysics scheme (WSM6). *J. Korean Meteorol. Soc.* 42: 129–151.
- Hong, S.Y. and Noh, Y. (2006). A new vertical diffusion package with an explicit treatment of entrainment processes. *Mon. Weather Rev.* 134: 2318–2341.
- Hung, C.H. and Lo, K.C. (2015). Relationships between ambient ozone concentration changes in Southwestern Taiwan and invasion tracks of tropical typhoons. *Adv. Meteorol.* 2015: 402976.
- Kumar, A., Patill, R.S., Dikshit, A.K. and Kumar, R. (2017). Application of WRF model for air quality

- modelling and AERMOD – A survey. *Aerosol Air Qual. Res.* 17: 1925–1937.
- Kumar, R., Naja, M., Pfister, G.G., Barth, M.C., Wiedinmyer, C. and Brasseur, G.P. (2012). Simulations over South Asia using the weather research and forecasting model with chemistry (WRF-Chem): Chemistry evaluation and initial results. *Geosci. Model Dev.* 5: 619–648.
- Kurokawa, J., Ohara, T., Morikawa, T., Hanayama, S., Greet, J.M., Fukui, T., Kawashima, K. and Akimoto, H. (2013). Emissions of air pollutants and greenhouse gases over Asian regions during 2000–2008: Regional Emission inventory in ASIA (REAS) version 2. *Atmos. Chem. Phys.* 13: 10049–10123.
- Lacono, M.J., Delamere, J.S., Mlawer, E.J., Shephard, M.W., Clough, S.A. and Collins, W.D. (2008). Radiative forcing by long-lived greenhouse gases: Calculations with the AER radiative transfer models. *J. Geophys. Res.* 113: D13103.
- Li, T.C., Chen, W.H., Yuan, C.S., Wu, S.P. and Wang, X.H. (2013). Physicochemical characteristics and source apportionment of atmospheric particles in Kinmen-Xiamen Archipelago. *Aerosol Air Qual. Res.* 13: 308–323.
- Li, T.C., Yuan, C.S., Lo, K.C., Hung, C.H., Wu, S.P. and Tong, C. (2015). Seasonal variation and chemical characteristics of atmospheric particles at three islands in the Taiwan Strait. *Aerosol Air Qual. Res.* 15: 2277–2290.
- Liu, X.Y., Zhang, Y., Zhang, Q. and He, K.B. (2016). Application of online-coupled WRF/Chem-MADRID in East Asia: Model evaluation and climatic effects of anthropogenic aerosols. *Atmos. Environ.* 124: 321–336.
- Lo, K.C. and Hung, C.H. (2012). The Development and Application of Weather Research Forecast Chemistry model. *Int. J. Appl. Comput. Technol.* 4: 138–144.
- Lu, H.C., Chang, C.L. and Hsieh, J.C. (2006). Classification of PM₁₀ distributions in Taiwan. *Atmos. Environ.* 40: 1452–1463.
- Morrison, H., Thompson, G. and Tatarskii, V. (2009). Impact of cloud microphysics on the development of trailing stratiform precipitation in a simulated squall line: Comparison of one- and two moment schemes. *Mon. Weather Rev.* 137: 991–1007.
- Nenes, A., Krom, M.D., Mihalopoulos, N., Cappellen, P.V., Shi, Z., Bougiatioti, A., Zarmpas, P. and Herut, B. (2011). Atmospheric acidification of mineral aerosols: A source of bioavailable phosphorus for the oceans. *Atmos. Chem. Phys.* 11: 6265–6272.
- Pai, P., Vijayaraghavan, K. and Seigneur, C. (2000). Particulate matter modeling in the Los Angeles basin using SAQM-AERO. *J. Air Waste Manage. Assoc.* 50: 32–42.
- Saikawa, E., Kim, H., Zhong, M., Avramov, A., Zhao, Y., Janssens-Maenhout, G., Kurokawa, J., Klimont, Z., Wagner, F., Naik, V., Horowitz, L.W. and Zhang, Q. (2017). Comparison of emissions inventories of anthropogenic air pollutants and greenhouse gases in China. *Atmos. Chem. Phys.* 17: 6393–6241.
- Shrivastava, M., Fast, J.D., Easter, R., Gustafson, W.I., Zaveri, R., Jimenez, J.L., Saide, P. and Hodzic, A. (2011). Modeling organic aerosols in a megacity: Comparison of simple and complex representations of the volatility basis set approach. *Atmos. Chem. Phys.* 11: 6639–6662.
- Streets, D.G., Bond, T.C., Carmichael, G.R., Fernandes, S.D., Fu, Q., He, D., Klimont, Z., Nelson, S.M., Tsai, N.Y., Wang, M.Q., Woo, J.H. and Yarber, K.F. (2003). An inventory of gaseous and primary aerosol emissions in Asia in the year 2000. *J. Geophys. Res.* 108: 8809–8831.
- Taiwan EPA (2016). *Taiwan emission data system 9.0*. Taiwan Environment Protection Administration. Taipei, Taiwan.
- Tie, X.X., Madronich, S., Walters, S., Zhang, R., Rasch, P.J. and Collins, W. (2003). Effect of clouds on photolysis and oxidants in the troposphere. *J. Geophys. Res. Atmos.* 108: 4642.
- Wang, L.T., Liu, Z., Sun, Y., Ji, D. and Wang, Y. (2015). Long-range transport and regional sources of pm_{2.5} in Beijing based on long-term observations from 2005 to 2010. *Atmos. Res.* 157: 37–48.
- Wang, Z., Itahashi, S., Uno, I., Pan, X., Osada, K., Yamamoto, S., Nishizawa, T., Tamura, K. and Wang, Z. (2017). Modeling the long-range transport of particulate matters for January in East Asia using NAQPMS and CMAQ. *Aerosol Air Qual. Res.* 17: 3064–3078.
- Wu, S.P., Schwab, J., Liu, B.L., Li, T.C. and Yuan, C.S. (2015). Seasonal variations and source identification of selected organic acids associated with PM₁₀ in the coastal area of Southeastern China. *Atmos. Res.* 155: 37–51.
- Yamartino, R.J., Scire, J.S., Charmichael, G.R. and Chang, Y.S. (1992). The CALGRID mesoscale photochemical grid model—I. Model formulation. *Atmos. Environ.* 26: 1493–1512.
- Yang, J., Kang, S. and Ji, Z. (2017). Sensitivity analysis of chemical mechanisms in the WRF-Chem model in reconstructing aerosol concentrations and optical properties in the Tibetan Plateau. *Aerosol Air Qual. Res.* 17: 505–521.
- Yen, M.C., Peng, C.M., Chen, T.C., Chen, C.S., Lin, N.H., Tzeng, R.Y., Lee, Y.A. and Lin, C.C. (2013). Climate and weather characteristics in association with the active fires in northern Southeast Asia and spring air pollution in Taiwan during 2010 7-SEAS/Dongsha Experiment. *Atmos. Environ.* 78: 35–50.
- Zhang, H., Xie, B., Zhao, S.Y. and Chen, Q. (2014). PM_{2.5} and tropospheric O₃ in China and an analysis of the impact of pollutant emission control. *Adv. Clim. Change Res.* 5: 136–141.
- Zhang, L., Cheng, Y., Zhang, Y., He, Y., Gu, Z. and Yu, C. (2017). Impact of air humidity fluctuation on the rise of PM mass concentration based on the high-resolution monitoring data. *Aerosol Air Qual. Res.* 17: 543–552.
- Zhang, Y., Liu, Y., Kucera, P.A., Alharbi, B.H., Pan, L. and Ghulam, A. (2015). Dust modeling over Saudi Arabia using WRF-Chem: March 2009 severe dust case. *Atmos. Environ.* 119: 118–130.
- Zhang, Y., Zhang, X., Wang, K., Zhang, Q., Duan, F. and He, K. (2016). Application of WRF/Chem over East Asia:

- Part II. Model improvement and sensitivity simulations. *Atmos. Environ.* 124: 301–320.
- Zhang, Y., Zhang, X., Wang, L., Zhang, Q., Duan, F. and He, K. (2016). Application of WRF/Chem over East Asia: Part I. Model evaluation and intercomparison with MM5/CMAQ. *Atmos. Environ.* 124: 285–300.
- Zheng, J., Che, W., Zheng, Z., Chen, L. and Zhong, L. (2013). Analysis of spatial and temporal variability of PM₁₀ concentrations using MODIS aerosol optical thickness in the Pearl River Delta region, China. *Aerosol Air Qual. Res.* 13: 862–876.
- Zheng, M., Salmon, L.G., Schauer, J.J., Zeng, L., Kiang, C.S., Zhang, Y. and Cass, G.R. (2005). Seasonal trends in PM_{2.5} source contributions in Beijing, China. *Atmos. Environ.* 39: 3967–3976.

Received for review, December 2, 2017

Revised, January 30, 2018

Accepted, January 31, 2018